

<https://doi.org/10.1038/s41612-024-00868-y>

Aerosol forces mesoscale secondary circulations occurrence: evidence of emission reduction

Check for updates

Jixiang Li^{1,2}, Haipeng Yu¹✉, Markku Kulmala ^{3,4,5}, Tom V. Kokkonen ³, Kai Tang ^{6,7}, Jianmin Ma ², Zeyong Hu¹, Siyu Chen ⁸, Yuling Hu¹, Rong Dai², Bofei Zhang¹, Hongyu Luo¹ & Shu Tao ²

Here, we present modeling evidence of the influences of aerosol feedback on secondary circulations (SCs). The results show that in heavily PM_{2.5} polluted Beijing-Tianjin-Hebei (BTH) areas, the aerosol feedback is the primary factor on the occurrence and development of mesoscale SCs in the atmospheric boundary layer. Modeling evidence reveal that the impact of aerosol feedback on SCs is proportional to PM_{2.5} concentrations or precursor emissions. During the 2014 Asia-Pacific Economic Cooperation (APEC) with extraordinary emission reduction, the time levels of SCs significantly decreases to ~37.3% of the periods without emission reduction before and after APEC period. The simulated PM_{2.5} during APEC are ~47.6% of before and after APEC period, and the measured concentration ratio at 47.7%. The largest variation in SC occurred during the afternoon, which should be related to the stronger solar radiation. We found that the reduction in wind speed caused by aerosol feedback and related convergence and divergence of the air mass play a pivotal role in SCs evolution. Against the background of prevailing westerly winds in BTH, the strengthening and appearance of clockwise SCs caused by aerosol feedback leads to an increase in the frequency of surface easterly U-wind. These phenomena have also been validated in two other emission reduction events and the emission reduction actions in the BTH region in January and July of 2014, 2017, and 2020, respectively. The results of this paper showing substantial impact of aerosol feedback on SCs, which could help promote our understanding of content and level of aerosol feedback to atmospheric changes.

Aerosols play an important role in the radiative balance of the Earth's atmosphere system, making it crucial to quantify the changes in radiation and heat budget caused by aerosols for a better understanding of synoptic or climate variations¹. Aerosol feedback can reduce solar radiation and planetary boundary layer (PBL) wind speeds^{2–4}, alter horizontal and vertical wind speeds^{5,6}, and cause abnormal cyclonic circulations^{7–9}, and pose a threat to human health¹⁰. The climatic effects of aerosols have raised widespread concerns in the scientific communities^{11–14}. However, there are

few studies based on dynamics, especially lacking in research on whether it will lead to the appearance of secondary circulation (SC). SC plays a vital role in atmospheric motion^{15,16}, and it is always associated with synoptic processes and microclimate to some extent^{17–19}. In addition, due to the complexity of the synoptic or climatic system and the interactions between atmospheric pollutants and synoptic/climatic systems, assessing the aerosol impact on climate is still a challenge under the current polluted air conditions^{20–23}.

¹Key Laboratory of Cryospheric Science and Frozen Soil Engineering, Nagqu Plateau Climate and Environment Observation and Research Station of Tibet Autonomous Region, Northwest Institute of Eco-Environment and Resources, Chinese Academy of Sciences, Lanzhou, China. ²Laboratory for Earth Surface Processes, College of Urban and Environmental Sciences, Peking University, Beijing, China. ³Institute for Atmospheric and Earth System Research (INAR)/Physics, University of Helsinki, Helsinki, Finland. ⁴Aerosol and Haze Laboratory, Beijing Advanced Innovation Center for Soft Matter Science and Engineering, Beijing University of Chemical Technology, Beijing, China. ⁵Joint International Research Laboratory of Atmospheric and Earth System Sciences, School of Atmospheric Sciences, Nanjing University, Nanjing, China. ⁶Project Management Office of China National Scientific Seafloor Observatory, Tongji University, Shanghai, China. ⁷Multiphase Chemistry Department, Max Planck Institute for Chemistry, Mainz, Germany. ⁸Key Laboratory for Semi-Arid Climate Change of the Ministry of Education, College of Atmospheric Sciences, Lanzhou University, Lanzhou, China. ✉e-mail: yuhp@lzb.ac.cn

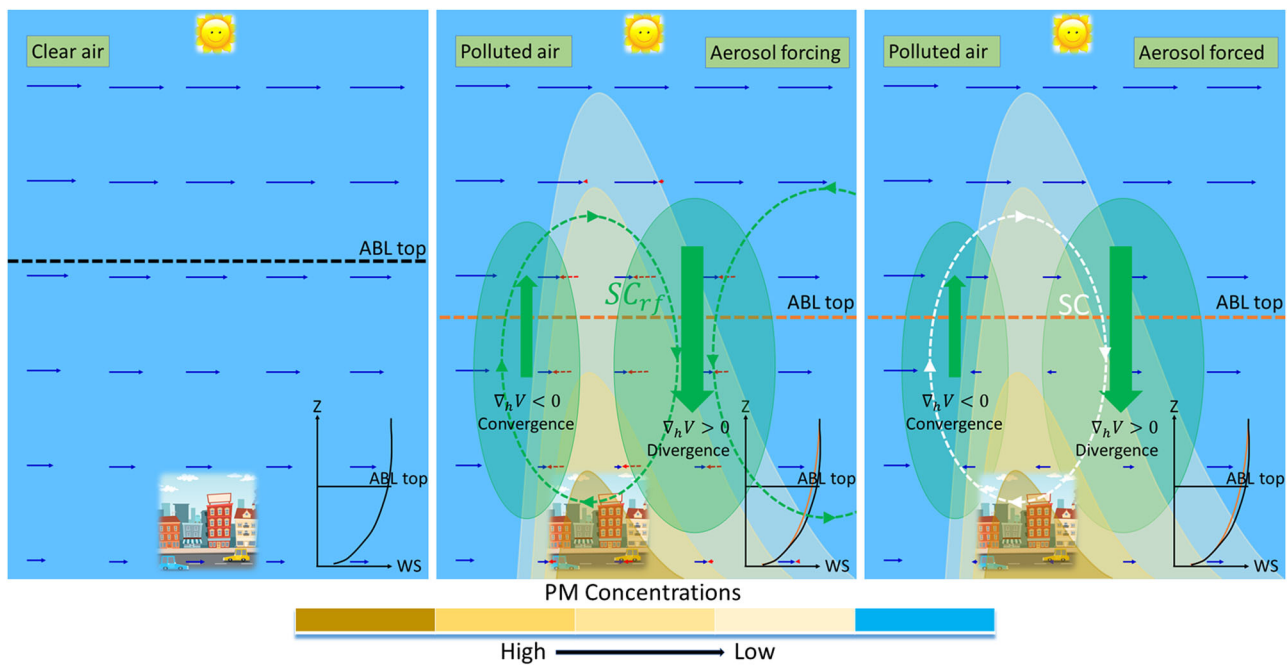


Fig. 1 | Schematic view of the mesoscale SCs evolution influenced by aerosol feedback effect in the atmospheric boundary layer. The green dashed circles are reinforced SCs, the white dashed circle is SC, the blue arrow lines denote wind speeds, and the dashed red arrow lines indicate the wind speed difference between feedback and non-feedback effect. The solid green thick arrow lines represent the

downward and upward motion induced by low atmospheric boundary layer (ABL) divergence or convergence. The shaded color region stands for PM concentrations and $\nabla_h V$ is horizontal divergence (s^{-1} , $\text{div} = -\nabla_h \vec{V}$). Convergent and divergent areas caused by the feedback effects are marked as shallow green oval areas.

Here, we propose a two-way interaction dynamical mechanism between the SCs and PM concentrations. Figure 1 presents a schematic view of the SCs evolution (including the process of reinforced SC forming and SC occurrence) influenced by aerosol feedback. Suppose that the region is under the westerly wind regime, since heavy aerosol pollution tends to reduce wind speed, the closer to the center of heavy pollution, the weaker the wind speed is. Consequently, the upstream area of the heavy pollution region forms a convergence zone, and the downstream area becomes a divergence zone, which would generate vertical motions to maintain mass conservation. Under favorable synoptic-scale background meteorological conditions, the downward and upward airflow strengthen further, leading to the formation of a convergence zone above the divergence zone. Eventually, a strong and well-structured clockwise rotating SC and a weaker counter-clockwise rotating SC are formed. But when the aerosol feedback impact is not very strong, often only the well-structured clockwise rotating SC appears.

Beijing-Tianjin-Hebei is one of the most severely polluted areas in China^{24,25}. The emission actions in Beijing-Tianjin-Hebei (BTH) and its surrounding regions during the 2014 Asia-Pacific Economic Cooperation (APEC) Summit in Beijing, resulted in a significant improvement in air quality, and the air tended to be cleaner^{26,27}. This provided unique data and scenarios for better understanding of the impact of particulate matter^{28,29} on SC. To further verify the reliability of the results, two emission reduction events in 2015 and 2017 in the BTH³⁰ were also selected. Due to the implementation of emission policies in recent years, PM_{2.5} concentrations have been declining^{31,32}. Therefore, January and July of 2014, 2017, and 2020 were selected as the validation of long-term emission reduction policies, rather than emission reduction events. WRF-Chem model was used to simulate the influence of aerosol feedback on SC, further details of model setup in methods.

Results and discussion

Association between PM_{2.5} and SCs

On the heavily polluted day closest before APEC without emission reduction (BAPEC, Supplementary Table 2), in the morning of October 30th

(Fig. 2a), the planetary boundary layer height (PBLH) was low and the ground-level PM_{2.5} concentrations were high. A clockwise rotating SC can be identified in the vicinity of Beijing with a horizontal scale of about 100 km and a vertical scale of about 1 km. Due to the upward transport by the SC, a high PM_{2.5} plum occurred in the western side of SC. In the afternoon (Fig. 2b), SC still maintained, on a larger spatial scale compared to the morning, PM_{2.5} concentrations continued to rise as they were not easily dispersed. By evening (Fig. 2c), the SC weakened and shifted eastward, resulting in a decrease in ground-level concentrations in the Beijing area. At night (Fig. 2d), SC further weakened and PM_{2.5} concentration continued to decrease. On the most severe heavily polluted day during APEC with emission reduction (DAPEC), in the morning of November 4th (Fig. 2e), there was a SC, but its structure was not as clear as that of the morning in BAPEC, and PM_{2.5} concentrations were low. In the afternoon (Fig. 2f), only one smaller and weaker scale SC occurred compared to the morning. PM_{2.5} was notably smaller than those in the BAPEC. In the evening (Fig. 2g) and at night (Fig. 2h), SC was not detectable, and PM_{2.5} concentrations were significantly lower than that of BAPEC. On the heavily polluted day closest after APEC without emission reduction (AAPEC), in the morning of November 15th (Fig. 2i), a smaller SC can be discerned. In the afternoon (Fig. 2j), a well-defined and larger-scale SC occurred. In the evening (Fig. 2k), the SC further intensified. But at night (Fig. 2l), SC weakened and PM_{2.5} concentration decreased.

The mesoscale SC mainly occurs in the region to the flat area and below 2 km altitude in the vertical direction. The SC during DAPEC was significantly weakened with the evolution from its occurrence in the morning, weakening at afternoon, and vanishing in the evening and night. In contrast, during BAPEC and AAPEC, SC also strengthened throughout the daytime. PM_{2.5} pollution during DAPEC was significantly lower than that during BAPEC and AAPEC, indicating a strong relationship between the PM_{2.5} levels and mesoscale SCs.

We use the time levels to represent how many times the SC could be identified in specific hour in specific period. The time levels of SCs (Fig. 3a) during DAPEC significantly decrease to ~37.3% of the periods during BAPEC and AAPEC (Supplementary Table 9). The simulated PM_{2.5}

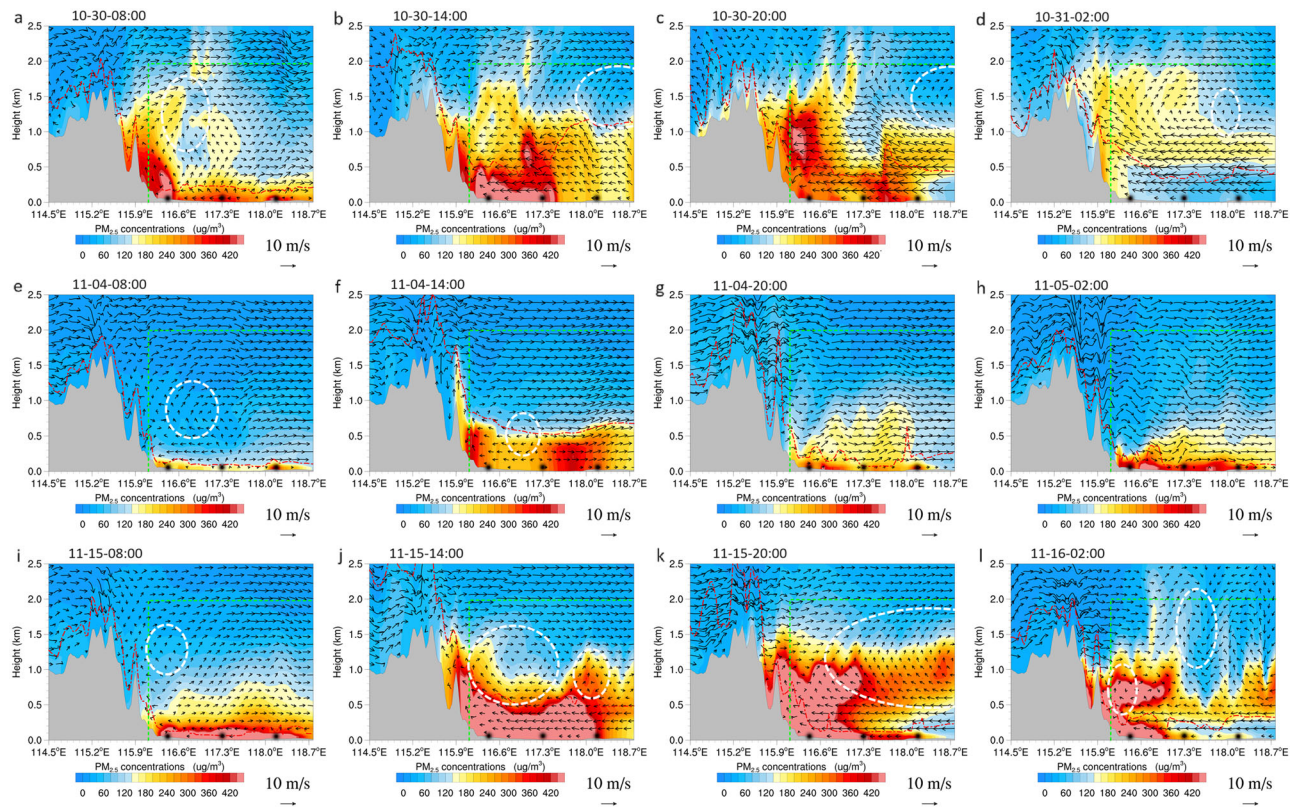


Fig. 2 | Feedback simulation of vertical cross-section of modeled hourly resultant vector winds ($U-W$, $m s^{-1}$) and $PM_{2.5}$ concentrations in three representative heavily polluted days. **a 08:00 LST, October 30th in BAPEC, **b** same as **a** but for 14:00 LST, **c** same as **a** but for 20:00 LST, **d** same as **a** but for 02:00 LST, October 31st, **e** 08:00 LST November 4th in DAPEC, **f** same as **e** but for 14:00 LST, **g** same as **e** but for 20:00 LST, **h** same as **e** but for 02:00 LST, November 5th, **i** 08:00 LST November**

15th in AAPEC, **j** same as **i** but for 14:00 LST, **k** same as **i** but for 20:00 LST, **l** same as **i** but for 02:00 LST, November 16th. The red solid line denotes the PBLH. The white dashed circles highlight SCs, and the green dashed line is the region to the flat area (east of the 47th grid point) and below 2 km altitude in the vertical direction. The three black dots from left to right on the bottom of each figure stand for the positions of BJP, BTP, and TSP, respectively (Supplementary Table 3).

(Fig. 3b) during DAPEC are $\sim 47.6\%$ of BAPEC and AAPEC, and the measured concentration ratio at 47.7% . We further used the mean value of $U-W$ vorticity ($Vorj$, $10^{-3} s^{-1}$) on vertical profile to quantify the occurrence and strength of SC and set a threshold value of $3.0 \times 10^{-3} s^{-1}$ to measure changes in SC. We found that the absolute value of $Vorj$ ($Vorj_Abs$) averaged over DAPEC reduced by 52.8% from BAPEC and AAPEC (Fig. 3c). And the result reveals that the accuracy of SC occurrence determined by vorticity (Fig. 3d) compared to manual identification was 79.2% . During DAPEC, $PM_{2.5}$ concentrations, its precursors (e.g., NO , SO_2 , and TOL) and $Vorj_Abs$ all decreased compared to the BAPEC and AAPEC, and their trends over time were quite similar (Supplementary Fig. 2).

Compared to the feedback simulation, the time levels of SCs are slightly lower in the non-feedback simulation (Supplementary Fig. 3, Table 10), and the largest variation in SC numbers occurred during the afternoon, which should be related to the stronger solar radiation in that afternoon (Supplementary Table 11). Since aerosol feedback acts directly to alter radiation^{33,34}, the stronger incoming radiation in afternoon leads to a greater forcing aerosol effect on SC, and it should even induce the occurrence of SC. The results indicate that SC is likely to be reinforced during periods with high $PM_{2.5}$ concentrations and stronger radiation.

During the other two emission reduction events in 2015 and 2017 (Supplementary Fig. 4), $PM_{2.5}$ concentrations and the number of identified SCs significantly decreased during the emission reduction period, compared to the before and after periods without emission reduction. In addition, $PM_{2.5}$ precursors concentrations (e.g., NO , SO_2 , and TOL) and $Vorj_Abs$ are all decreased during the emission reduction period, and their trends were also quite similar (Supplementary Figs. 5 and 6). For all the times of three emission reduction events (Fig. 3e-i), the time levels of SCs occurrence measured by $Vorj$, $PM_{2.5}$ concentrations, and $Vorj_Abs$ were significantly

decreased during emission reduction period. Moreover, the surface U -wind direction also shows changes corresponding to the number of SCs or $U-W$ vorticity. The main manifestation is that after the strengthening of SCs by aerosol feedback, the frequency of easterly U -winds increases, except for the D_15ER period of observed winds, which should be related to the background wind field not being dominated by westerly winds. Since in recent years, most of $PM_{2.5}$ are secondary in Beijing. Moreover, we also noticed that the average proportion of secondary aerosols for the all times during the 2014 APEC events was 59.2% , and the proportion above 70% often occurred (Supplementary Fig. 7), the correlation coefficient between $Vorj$ and secondary $PM_{2.5}$ ($R = 0.239$, which passed the two-tailed significance T-tests, $P < 1.0 \times 10^{-10}$) exceeds the correlation coefficient with total $PM_{2.5}$ (0.227). However, the proportion of secondary $PM_{2.5}$ in the 2015 and 2017 reduction events was not high, which should be due to the higher proportion as winter approached^{23,35}. In winter, secondary aerosols may have a better correlation with SC.

From 2014 to 2020 when emission reduction actions were taken³⁶, the emissions of $PM_{2.5}$ and its precursors (SO_2 , NO_x , VOC , and NH_3) have also shown a downward trend, and the observed concentration of $PM_{2.5}$ has also decreased (Supplementary Fig. 8). The time levels of SCs occurrence by $Vorj$, $PM_{2.5}$ concentrations, and $Vorj_Abs$ were decreased in January and July from 2014 to 2017 and then to 2020 (Fig. 3j-n), and $PM_{2.5}$ precursors concentrations (e.g., NO , SO_2 , and TOL) also decreased (Supplementary Figs. 9 and 10). The surface U -wind direction also shows changes corresponding to the number of SCs or $U-W$ vorticity (Fig. 3m, n). But the relationship between simulated wind and SC is not better than observed, that should be because the input data for WRF are once every 6 h, which cannot more accurately reflect the hourly variation of surface wind like the observed hourly data. Additionally, some inconsistencies should originate from the background wind field.

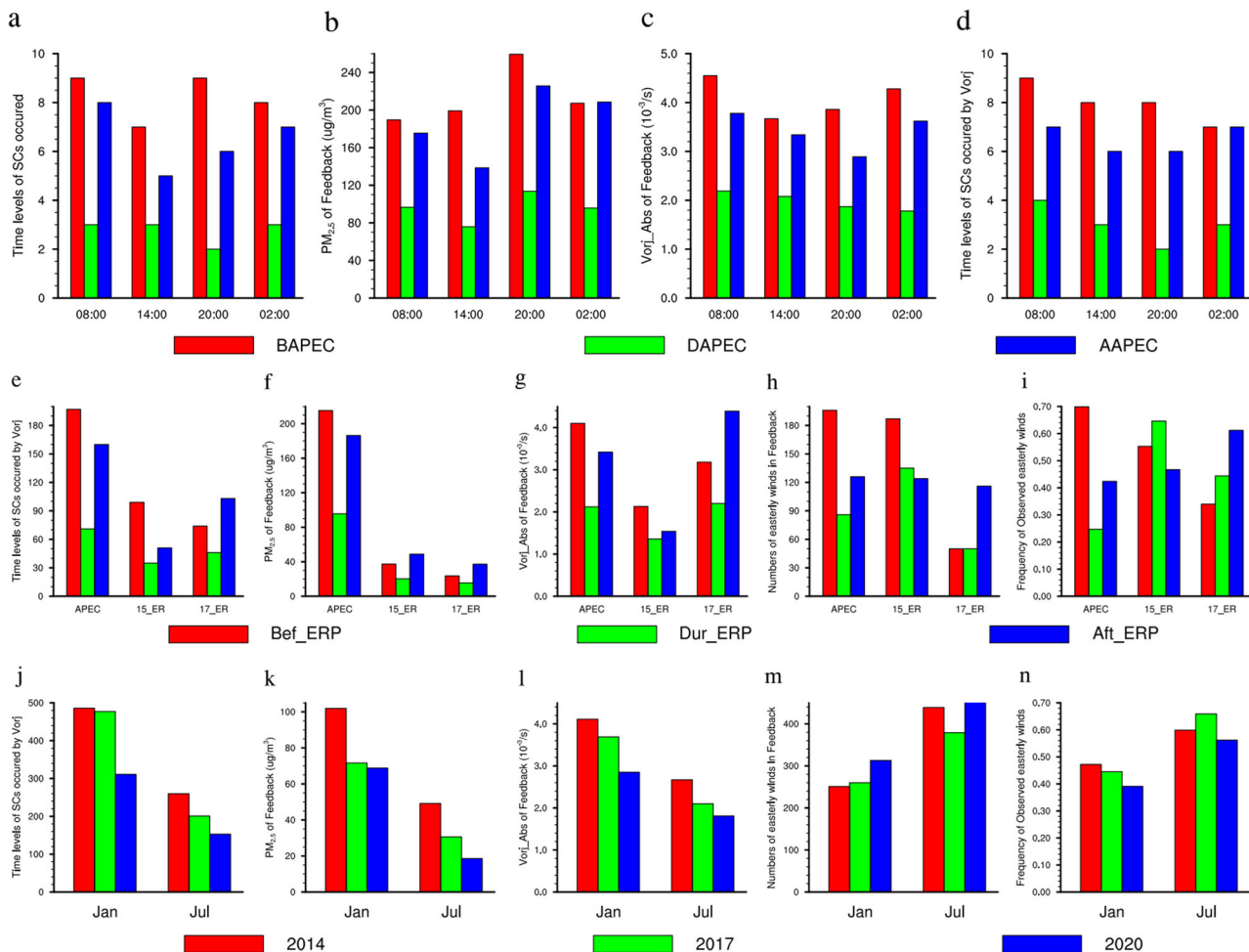


Fig. 3 | Statistical data on variables related to secondary circulation in the Feedback simulation. **a** Time levels with the occurrence of mesoscale SCs, during BAPEC, DAPEC, and AAPEC at 08:00 LST, 14:00 LST, 20:00 LST, and 02:00 LST, **b** same as **a** but for simulated $PM_{2.5}$ concentrations, **c** same as **a** but for simulated Vorj_Abs, **d** same as **a** but for the number of hours with the occurrence of mesoscale SCs judged by Vorj, **e** time levels with the occurrence of mesoscale SCs judged by Vorj, before and after the emission reduction period in 2014 APEC, 2015 and

2017 events, **f** same as **e** but for simulated $PM_{2.5}$ concentrations, **g** same as **e** but for simulated Vorj_Abs, **h** same as **e** but for the numbers of easterly U-winds, **i** same as **e** but for the frequency of observed easterly U-winds, **j** time levels with the occurrence of mesoscale SCs judged by Vorj, in January and July of 2014, 2017 and 2020, **k** same as **j** but for simulated $PM_{2.5}$ concentrations, **l** same as **j** but for simulated Vorj_Abs, **m** same as **j** but for the numbers of easterly U-winds, **n** same as **j** but for the frequency of observed easterly U-winds.

Potential mechanism of aerosol feedback influence on SCs

During the heavily polluted days (Fig. 4a–k), reinforced SCs caused by aerosol feedback can be clearly discerned at each time. Comparing DAPEC with the other two periods, the vertical wind speed is significantly lower, resulting in weaker reinforced SCs in wind speed and smaller scales in spatial structure. When the westerly wind (Fig. 2f–i) prevails, the reinforced SCs result in convergence and divergence in the downwind areas of high $PM_{2.5}$ concentrations (upper right in Fig. 4f–i). When the predominant wind direction is easterly, due to the blocking effect of Beijing's Western Hills on aerosols, high concentrations primarily accumulate at the foothills of the Western Hills and do not significantly transport downstream^{37,38} (Fig. 4a–c, g, k), resulting in a strong convergence zone in the upstream region due to the reduction in wind speed, along with the forced upward flow due to the blocking effect of the mountains. This leads to the occurrence of a strong reinforced SC in the upstream region (upper right in Fig. 4a–c, g, k). However, in the downstream region where the high concentration decreases, which is difficult for a mesoscale SC with a certain spatial scale to be reinforced. It means that the occurrence of reinforced mesoscale SC corresponds well with $PM_{2.5}$ concentrations. The reinforced SC generally appears in the upper right of areas with high $PM_{2.5}$ concentrations, which is in line with the mechanism for the impact of aerosol feedback on SCs (Fig. 1).

For the average over BAPEC and AAPEC, high $PM_{2.5}$ concentrations (Supplementary Fig. 11) correspond well with reinforced mesoscale SCs (Supplementary Fig. 12), but it is not straightforward to identify well-structured reinforced mesoscale SCs during DAPEC. Moreover, compared to the hourly U-W differences (Fig. 4), the SC structure averaged over the three periods (Supplementary Fig. 12) is more complete, with larger spatial scales and better correspondence with $PM_{2.5}$ concentrations. This is likely because the mean U and W winds averaged over the three periods filter out some incidental factors that may disturb SC, focusing mainly on the relationship between aerosol feedback and SCs.

Relationship between SC and synoptic background

Different synoptic background wind fields could result in different characteristics of reinforced SCs. When westerly flow prevailed (Fig. 4g, Supplementary Fig. 12a), there was a better match between the reinforced SCs and the conceptual SC (Fig. 1). When easterly background flow prevailed (Fig. 2b, c), the updrafts in the reinforced SCs were often stronger than the downdrafts. The reinforced SCs were primarily located near the top of PBL and were associated with areas with high $PM_{2.5}$ concentrations. The SC occurred is the result of the combined effect of background and reinforced SC. The synoptic charts (500-hPa, 850-hPa, surface, and surface wind field map, Supplementary Figs. 13–18) indicate that the synoptic situation were

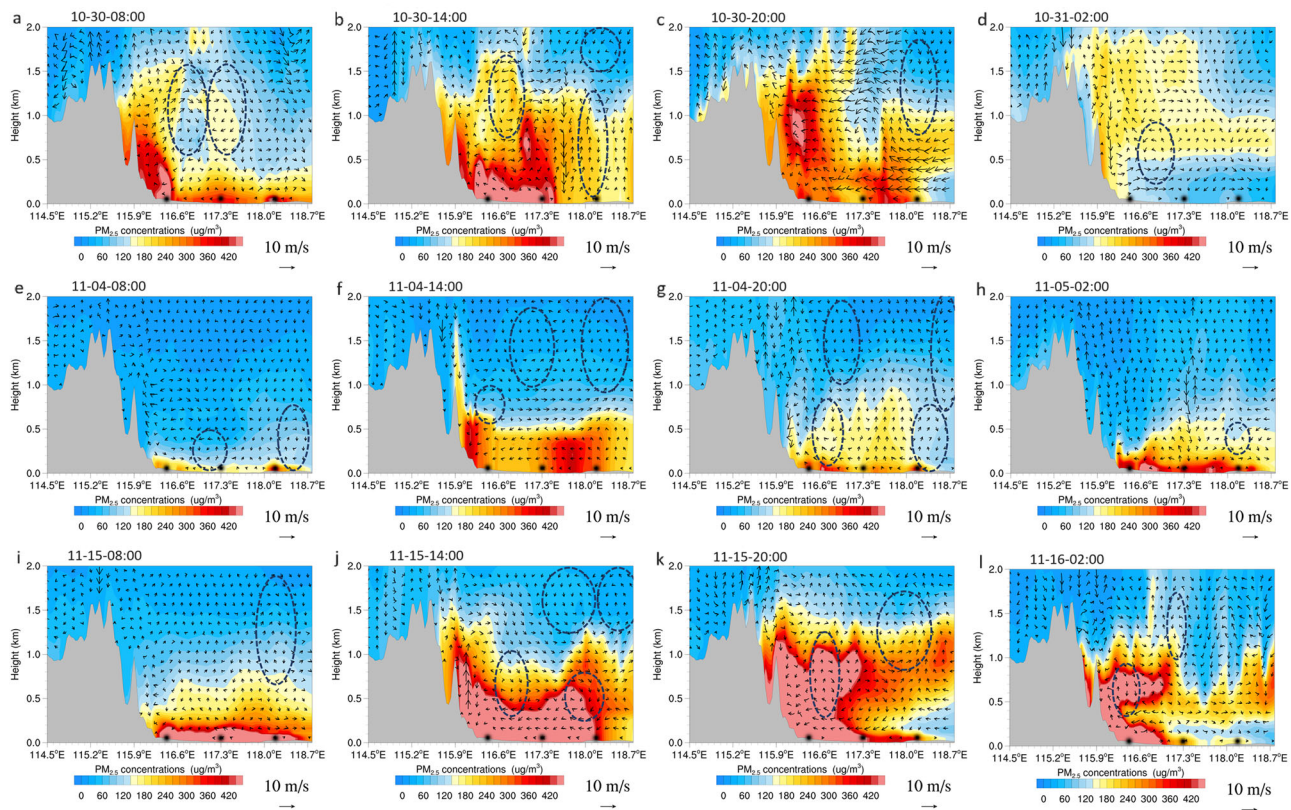


Fig. 4 | Vertical cross-sections of differences of hourly U-W wind vectors between feedback and non-feedback simulations and $\text{PM}_{2.5}$ concentrations from feedback simulations in three representative heavily polluted days. a 08:00 LST, October 30th in BAPEC, **b** same as **a** but for 14:00 LST, **c** same as **a** but for 20:00 LST, **d** same as **a** but for 02:00 LST, October 31st, **e** 08:00 LST November 4th in DAPEC, **f** same as

e but for 14:00 LST, **g** same as **e** but for 20:00 LST, **h** same as **e** but for 02:00 LST, November 5th, **i** 08:00 LST November 15th in AAPEC, **j** same as **i** but for 14:00 LST, **k** same as **i** but for 20:00 LST, **l** same as **i** but for 02:00 LST November 16th. The blue dashed circles highlight reinforced SCs. The three black dots on the abscissa denote, respectively, BJT, BTP, and TSP from left to right (Supplementary Table 3).

not the primary cause of SCs and its vertical motion at the low atmosphere (Supplementary Information provide details). Although trough and surface convergence should contribute to high concentrations and evolution of SCs^{37,39,40}. Comparing the feedback and non-feedback simulations, we can identify similarities of hourly wind fields as well as geopotential heights and temperatures (Supplementary Figs. 19–22). As some studies have previously pointed out, the impact of aerosol feedback on wind field is about an order of magnitude smaller than that of the background wind field^{2,41,42}. This is consistent with the average situation (Supplementary Fig. 12) of our research. However, on hourly basis, the impact of aerosol feedback on wind field is of the same order of magnitude as the background wind field (Figs. 2 and 4). Furthermore, the R between Vorj and meteorological scalar fields (e.g., Div, wind speed and its gradient and temperature and its gradient, etc. Supplementary Tables 12–16) are notably lower than those for $\text{PM}_{2.5}$ and Vorj. Notably, the R between Vorj below 1 km and $\text{PM}_{2.5}$ reaches up to 0.717 ($P < 0.001$) in afternoon. This suggests that while synoptic background does influence the location and characteristics of SC, aerosol impact should be the primary factor associated with SC occurrence.

The statistical results (Fig. 3h, i, m, n) show that the influence of background meteorological fields on SCs is also very important. In the BTH area, the upper atmosphere (e.g., 500-hpa, Supplementary Figs. 13, 14, 23, 24) is mainly dominated by westerly winds^{43,44}, but the prevailing wind direction near the top of the boundary layer (e.g., 850-hpa, Supplementary Figs. 15, 25, 26) and on the surface may not necessarily be mainly westerly (Supplementary Figs. 16–18, 27–31). When the dominant wind direction of the background is westerly (Supplementary Figs. 16, 27d–f, 30a–c), the SC generated by aerosol feedback is clockwise, resulting in an increase in the frequency of surface easterly U-winds, and when easterly winds prevail on the surface (Supplementary Figs. 27b, d, 30e, f), it will result in a decrease in

the frequency of surface easterly U-winds. For example, westerly winds are prevalent on the surface and 500-hpa in 2014 APEC and 2017 emission reduction events, during the emission reduction period, SC decreases and the frequency of easterly U-winds decreases. For January 2014, 2017 and 2020, modeled wind direction is easterly but observed as westerly, so the frequency of easterly U-winds increases in modeled but decreases in observed. Although there is a change in wind direction on the surface opposite to the background, which is not as good as the correlation between $\text{PM}_{2.5}$ and SC. However, for most periods, the observed wind corresponds better to the simulated SC than the simulated wind, which should be attributed to the fact that the observed wind speed contains more information about hourly variations.

In summary, heavy $\text{PM}_{2.5}$ pollution-induced aerosol feedback significantly enhances the evolution of mesoscale SCs, especially when solar radiation is strongest. It is primarily the aerosol feedback that serves as the main factor driving SC occurrences, although the synoptic background influences the location and characteristics of SC, and the frequency of surface U-winds opposite to the prevailing background wind associated with the change of SCs by aerosol feedback. SCs are constrained by surface, meteorological, dynamic, and thermodynamic conditions within the PBL⁴⁵. The locations and sizes of SCs associated with aerosol concentration distribution under aerosol feedback. Since our proposed two-way interaction dynamical mechanism between the SCs and PM concentrations, is based on the universal phenomenon of aerosol reducing wind speed and constrained by the law of conservation of air mass, the relevant conclusions should also have some reference significance in other places.

However, there are still uncertainties in the impact of aerosol feedback on weather or climate, such as aerosol-cloud interactions⁴⁶, the uncertainties in pollutant emission inventories⁴⁷ and WRF input data which contain

limited hourly meteorological variations. Additionally, the mechanism we proposed is the main process by which aerosols affect SCs, rather than the full chain of events associated with the feedback. The non-feedback simulation suggests that at least half of SCs should be attributed to the aerosol feedback effects during APEC non-emission reduction period. The observed PM_{2.5} and wind direction have a better correspondence with the simulated SC or U-W vorticity than the simulated PM_{2.5} and wind direction. These imply that the WRF-Chem model has shortcomings and might underestimate the impact of aerosol feedback⁴⁸ on SCs. Additionally, since the observed atmosphere is already polluted rather than clean air, the measured meteorological conditions might be subject to polluted air. As a result, the impact of anthropogenic aerosols on mesoscale SCs are likely to be more severe than the present research results. Despite significant efforts to improve air quality, air pollution in China continues to be a major environmental concern⁴⁹. The emergence of SCs caused by aerosol feedback may disturb the weather system, especially under heavy pollution conditions, which may increase the uncertainty of weather simulation. There should be many aspects that need to be studied in the two-way interactions between aerosols and meteorology and associated feedback^{6,11,48,50}. The better we understand aerosol feedback, the more effectively we can mitigate air pollution as well as mitigate climate forces and adapt to climate change.

Methods

Data introduction

The final operational global analysis data from national centers for environmental prediction (NCEP-FNL) with a resolution of 1° × 1° and a 6-h interval, were used to generate boundaries and initial conditions for WRF-Chem. The MEIC emission inventory for China was utilized, which has a resolution of 0.25° × 0.25° lat/lon⁵¹. The present study also incorporated MEGAN biogenic emissions data⁵² and biomass burning emissions data¹⁴. The initial conditions and boundary conditions for pollutant concentrations in each simulation were provided by the global model MOZART⁵³. The meteorological observation data are sourced from National Oceanic and Atmospheric Administration Integrated Surface Database (ISD-Lite). Pollutant monitoring data are obtained from the National Urban Air Quality Real-time Release Platform (<https://air.cnemc.cn:18007/>), which collects hourly PM_{2.5} concentration data. A total of 48 pollution monitoring sites within the model Domain 3 were selected and the site locations and names are provided in Supplementary Table 1.

During the APEC, extraordinary emission reduction measures were implemented in key regions (including BTH region and the western part of Shandong Province, including Liao Cheng, Dezhou, Jinan, Binzhou, Dongying, and Zibo, as delineated by the blue boundary line in Supplementary Fig. 1a). Significant changes in pollutant emissions occurred during the DAPEC period. The emission reduction ratios for various pollutants during the DAPEC period were referred to relevant literatures^{27,54}. The emission for PM_{2.5}, PM₁₀, SO₂, NO_x, NO₂, CO, and VOCs in Beijing were decreased by 39.2%, 66.6%, 61.6%, 49.6%, 39.9%, 28.8%, and 33.6%, respectively. Due to the lack of comprehensive emission reduction data for other key regions apart from Beijing, a rough estimate was made by assuming that the emission reduction ratios in Tianjin were 90% of those in Beijing, and for other regions, they were 80% of those in Beijing. In the emission reduction action from August 20 to September 3, 2015, the emission reduction ratios for PM_{2.5}, PM₁₀, SO₂, NO_x, NO₂, CO, and VOCs in Beijing were 73.0%, 69.0%, 46.0%, 52.0%, 52.0%, 38.0%, and 53.0%, respectively. In the emission reduction action from May 5 to 15, 2017, the emission reduction ratios for PM_{2.5}, PM₁₀, SO₂, NO_x, NO₂, CO, and VOCs in Beijing were 40.0%, 25.0%, 25.0%, 25.0%, 25.0%, 20.0%, and 25.0%, respectively. The emission reduction ratios of Tianjin were 90% of those in Beijing, and for other regions, they were 80% of those in Beijing for both emission reduction events.

Model setup

The WRF-Chem 4.1.3 version, a regional air quality model that fully couples meteorology and chemistry online⁵⁵, was used in this study. The Lambert projection was employed, and the model setup consisted of three nested

domains (Supplementary Fig. 1) with grid nesting ratios of 1:3:3. The horizontal resolutions and grid sizes for each domain were as follows: Domain 1: 27 km, 164 × 140 grids; Domain 2: 9 km, 156 × 153 grids; Domain 3: 3 km, 123 × 123 grids. Domain 1 covers the mainland of China, Domain 2 encompasses the North China Plain, Shanxi Province, parts of Shaanxi Province, and Inner Mongolia, and Domain 3 encircles Beijing, Tianjin, and surrounding areas. The model atmosphere has 28 vertical layers.

The physics parameterizations used in the model include the Morrison (2 moments) microphysics scheme⁵⁶, the Improved Rapid Radiative Transfer Model for General Circulation Models for longwave and shortwave radiation⁵⁷, the Monin-Obukhov surface layer scheme from MM5⁵⁸, the Unified Noah land-surface scheme⁵⁹, the MYNN 2.5 level Turbulence Kinetic Energy boundary layer scheme^{60,61}, and the Grell 3D ensemble cumulus parameterization with the Xu-Randall method for calculating cloud optical thickness⁶². The chemical module employed the MOZART mechanism⁶³, and the MOSAIC module with the KPP library is used for aerosol chemistry processes⁶⁴.

The simulation period extends from October 18th, 2014, 00:00 UTC to November 25th, 2014, 00:00 UTC, divided into three simulation periods, each lasting 14 days, in 2014 APEC. In the 2015 and 2017 emission reduction events, the simulation also divided into three simulation periods, each lasting 17 or 9 days, the period extends from August 3rd, 2015, 00:00 UTC to September 19th, 2015, 00:00 UTC, and from April 30th, 2017, 00:00 UTC to May 23th, 2017, 00:00 UTC, respectively. The starting time of each subsequent period is 2 days prior to the end time of the previous period. The first two days of each simulation period are designed as the spin-up period to allow the model's meteorological processes to reach a quasi-steady state. In the simulations conducted in January and July 2014, 2017, and 2020, each simulation lasted for 34 days, with the first three days used as the spin-up period and the remaining 31 days of each month used as the analysis data. The direct feedback of aerosols refers to their scattering and absorption of radiation, while the indirect feedback refers to the influence of aerosols on radiation after participating in cloud processes. In the feedback configuration, the bi-directional feedback mechanism between meteorology and pollutants was turned on, considering both direct and indirect effects of aerosols. While in the non-feedback configuration, both the direct and indirect feedback effects were turned off, and the cloud droplet concentration was set to a constant value of 250 cm⁻³^{3,24,65}.

Model simulations

This study investigates the impact of aerosol feedback on SC by comparing the simulation results of feedback and non-feedback configuration. The period from 08:00 LST on November 1st to 20:00 LST on November 12th, 2014, is considered as the APEC emission reduction period (referred to as DAPEC), while the period before APEC with the same duration (from 08:00 LST on October 20th to 20:00 LST on October 31st) is referred to as BAPEC, and the period after APEC with the same duration (from 08:00 LST on November 13th to 20:00 LST on November 24th) is referred to as AAPEC, respectively (Supplementary Table 2). Periods of other two emission reduction events are also listed in Supplementary Table 2. Considering that heavy air pollution occurs typically at the city scale, and the SC subject to aerosol feedback also should mainly occur at the city scale, the innermost nested domain (Domain 3) is selected for the study.

To visualize the SC, this study uses vertical cross-section diagrams that span Beijing and Tangshan cities along the Y-axis. The U-W composite wind vector profile is visualized by multiplying the vertical velocity W by 20 and then combining it with the U wind component (zonal wind) to highlight the influence of vertical velocity and better identify the boundary layer SC structure. We estimated the differences of meteorological variables and PM_{2.5} concentrations between feedback and non-feedback simulations at each time step. Three model grids were selected to plot wind profile: one located in the center of Beijing (referred to as BJP or the urban area), one in the center of Tangshan (referred to as TSP or the urban area), and one located between Beijing and Tangshan (referred to as BTP or the suburban

area). Of these grids, BTP is located 75 km east of BJP, and TSP is located 75 km east of BTP. Supplementary Fig. 1b shows the positions of the three grid points, and detailed information about their locations can be found in Supplementary Table 3. Detailed model verifications are presented in the Supporting Information (Supplementary Tables 4–7). Model validation shows that WRF-Chem demonstrates strong simulation capabilities in both feedback and non-feedback simulations^{66,67}, the simulation of PM_{2.5} and meteorological factors under feedback configuration is often better than that under non-feedback configuration, which also indicates the importance of aerosol feedback.

U-W vorticity, divergence, and gradient

Vorticity is defined as the curl of the velocity field and serves as a microscopic measure of fluid rotation characteristics. The spatial distribution of vorticity is referred to as the vorticity field, which is a vector field. Since SC mainly occurs in the flat area east of the Western Hills of Beijing in our study area, to eliminate the influence of the Western Hills on Vorj (Formulas in Supplementary Table 8), the U-W plane's average Vorj value was selected in the region to the east of the 47th grid point and below 2 km altitude in the vertical direction. To determine whether SC occurs by Vorj, we selected regions on the U-W plane with relatively flat topography. We consider the absolute mean value of Vorj greater than or equal to at threshold value of $3.0 \times 10^{-3}/s$ as the criterion for judging its presence. If the absolute value exceeds the threshold, secondary circulation is considered to be present. Otherwise, no SC occurs. The U-V divergence and vorticity and horizontal gradient of a scalar field were also calculated for the statistical testing of variables related to SC (Formulas in Supplementary Table 8).

The U-W vorticity (Vorj) was estimated using a central differencing scheme with second-order accuracy, where i and j represent i th grid along the east-west and j th level along vertical directions, respectively. mapfac_u and mapfac_w are the map factors for U and W. The vertical resolution Δz is 55 m, and the horizontal resolution Δx is 3000 m. Positive value of Vorj (1/s) indicates clockwise circulation and negative value of Vorj represents counterclockwise circulation. For the convenience of writing, the unit is set as $10^{-3}/s$ in this paper. The U-V divergence (Div, $10^{-5}/s$) and vorticity (Vor $10^{-5}/s$) were also estimated using a central differencing scheme with second-order accuracy, where mapfac_v is the map factors for V, and the horizontal resolution Δy is 3000 m. The horizontal gradient of a scalar field was calculated using a central differencing scheme with second-order accuracy, where mapfac_f is the map factors for f , these equations are used to calculate the gradients of meteorological scalar fields such as wind speed, temperature, and pressure (Formulas in Supplementary Table 8).

Data availability

Source codes of WRF-Chem model and model input geographical static data are available from the WRF website (https://www2.mmm.ucar.edu/wrf/users/download/get_source.html). All data sets used in this study are publicly available. Meteorological data were obtained from the NCEP Final Analysis website (<https://rda.ucar.edu/datasets/ds083.2/>). Monthly anthropogenic emissions are collected from MEIC v1.3 (http://meicmodel.org/?page_id=541&lang=en). MEGAN biogenic emissions data, biomass burning emissions data and the initial conditions and boundary conditions by MOZART are available at the WRF website (<https://www2.mmm.ucar.edu/wrf/users/download/>). Pollutant monitoring data are obtained from the National Urban Air Quality Real-time Release Platform (<https://air.cnemc.cn:18007/>). ISD-Lite meteorological observation data are sourced from the National Oceanic and Atmospheric Administration Integrated Surface Database (<https://www.ncei.noaa.gov/pub/data/noaa/isd-lite>).

Received: 10 July 2024; Accepted: 3 December 2024;

Published online: 19 December 2024

References

1. Kulmala, M. et al. Aerosols, clusters, greenhouse gases, trace gases and boundary-layer dynamics: on feedbacks and interactions. *Bound.-Layer. Meteorol.* **186**, 475–503 (2023).
2. Makar, P. A. et al. Feedbacks between air pollution and weather, Part 1: effects on weather. *Atmos. Environ.* **115**, 442–469 (2015).
3. Wang, H. et al. Mesoscale modelling study of the interactions between aerosols and PBL meteorology during a haze episode in China Jing-Jin-Ji and its near surrounding region—Part 2: aerosols' radiative feedback effects. *Atmos. Chem. Phys.* **15**, 3277–3287 (2015).
4. Albrecht, B. A. Aerosols, cloud microphysics, and fractional cloudiness. *Science* **245**, 1227–1230 (1989).
5. Li, Z. et al. Aerosol and boundary-layer interactions and impact on air quality. *Natl. Sci. Rev.* **4**, 810–833 (2017).
6. Abbott, T. H. & Cronin, T. W. Aerosol invigoration of atmospheric convection through increases in humidity. *Science* **371**, 83–85 (2020).
7. Menon, S., Hansen, J., Nazarenko, L. & Luo, Y. Climate effects of black carbon aerosols in China and India. *Science* **297**, 2250–2253 (2002).
8. Huang, X. et al. Smoke–weather interaction affects extreme wildfires in diverse coastal regions. *Science* **379**, 457–461 (2023).
9. Wang, Y., Zhang, R. & Saravanan, R. Asian pollution climatically modulates mid-latitude cyclones following hierarchical modelling and observational analysis. *Nat. Commun.* **5**, 3098 (2014).
10. Pozzer, A. et al. Mortality attributable to ambient air pollution: a review of global estimates. *Geohealth* **7**, e2022GH000711 (2023).
11. Charlson, R. J. et al. Climate forcing by anthropogenic aerosols. *Science* **255**, 423–430 (1992).
12. Ding, Y. et al. Atmospheric aerosols, air pollution and climate change. *Meteor Mon.* **35**, 3–14 (2009).
13. Ramanathan, V. & Carmichael, G. Global and regional climate changes due to black carbon. *Nat. Geosci.* **1**, 221–227 (2008).
14. Wiedinmyer, C., Yokelson, R. J. & Gullett, B. K. Global emissions of trace gases, particulate matter, and hazardous air pollutants from open burning of domestic waste. *Environ. Sci. Technol.* **48**, 9523–9530 (2014).
15. Shen, L., Sun, J., Yuan, R. & Liu, P. Characteristics of secondary circulations in the convective boundary layer over two-dimensional heterogeneous surfaces. *J. Meteorol. Res.* **30**, 944–960 (2017).
16. Bergmaier, P. T., Geerts, B., Campbell, L. S. & Steenburgh, W. J. The OWLeS IOP2b lake-effect snowstorm: dynamics of the secondary circulation. *Mon. Weather Rev.* **145**, 2437–2459 (2017).
17. Eder, F. et al. Secondary circulations at a solitary forest surrounded by semi-arid shrubland and their impact on eddy-covariance measurements. *Agric. For. Meteorol.* **211–212**, 115–127 (2015).
18. Kröniger, K. et al. Effect of secondary circulations on the surface–atmosphere exchange of energy at an isolated semi-arid forest. *Bound.-Layer. Meteorol.* **169**, 209–232 (2018).
19. Matinpour, H., Atkinson, J. & Bennett, S. Secondary circulation within a mixing box and its effect on turbulence. *Exp. Fluids* **61**, 225 (2020).
20. Carslaw, K. S. et al. Large contribution of natural aerosols to uncertainty in indirect forcing. *Nature* **503**, 67–71 (2013).
21. O'Connor, F. M. et al. Assessment of pre-industrial to present-day anthropogenic climate forcing in UKESM1. *Atmos. Chem. Phys.* **21**, 1211–1243 (2021).
22. William J. B. *Climate Change: A Multidisciplinary Approach* (Second Edition) 1–12 (Higher Education Press, 2010).
23. An, Z. et al. Severe haze in northern China: a synergy of anthropogenic emissions and atmospheric processes. *Proc. Natl. Acad. Sci. USA* **116**, 8657–8666 (2019).
24. Huang, R. J. et al. High secondary aerosol contribution to particulate pollution during haze events in China. *Nature* **514**, 218–222 (2014).
25. Wang, S. X. et al. Emission trends and mitigation options for air pollutants in East Asia. *Atmos. Chem. Phys.* **14**, 6571–6603 (2014).

26. Liu, J. G. et al. Haze observation and control measure evaluation in Jing-Jin-Ji (Beijing, Tianjin, Hebei) area during the period of the Asia-Pacific Economic Cooperation (APEC) meeting. *Bull. Chin. Acad. Sci.* **30**, 368–337 (2015).

27. Zhang, L. et al. Sources and processes affecting fine particulate matter pollution over North China: an adjoint analysis of the Beijing APEC period. *Environ. Sci. Technol.* **50**, 8731–8740 (2016).

28. Wang, H., Zhao, L., Xie, Y. & Hu, Q. APEC blue”—the effects and implications of joint pollution prevention and control program. *Sci. Total Environ.* **553**, 429–438 (2016).

29. Zhou, S. Long-term governance promotes “APEC Blue” to become the normal blue. *Environ. Prot.* **22**, 1 (2014).

30. Zhao, J. et al. Insights into aerosol chemistry during the 2015 China Victory Day parade: results from simultaneous measurements at ground level and 260 m in Beijing. *Atmos. Chem. Phys.* **17**, 3215–3232 (2017).

31. Zhang, Q., Zheng, Y., Tong, D., Shao, M. & Hao, J. Drivers of improved PM 2.5 air quality in China from 2013 to 2017. *Proc. Natl. Acad. Sci.* **116**, 201907956 (2019).

32. Wen, Z. et al. Combined short-term and long-term emission controls improve air quality sustainably in China. *Nat. Commun.* **15**, 5169 (2024).

33. Barbaro, E., Vilà-Guerau de Arellano, J., Krol, M. C. & Holtslag, A. A. M. Impacts of aerosol shortwave radiation absorption on the dynamics of an idealized convective atmospheric boundary layer. *Bound.-Layer. Meteorol.* **148**, 31–49 (2013).

34. Yu, S. et al. Aerosol indirect effect on the grid-scale clouds in the two-way coupled WRF–CMAQ: model description, development, evaluation and regional analysis. *Atmos. Chem. Phys.* **14**, 11247–11285 (2014).

35. Zhou, Y. et al. Variation of size-segregated particle number concentrations in wintertime Beijing. *Atmos. Chem. Phys.* **20**, 1201–1216 (2020).

36. Conibear L. et al. Emission sector impacts on air quality and public health in China from 2010–2020. *GeoHealth*, **6**, e2021GH000567 (2022).

37. Miao, Y. et al. Numerical study of the effects of local atmospheric circulations on a pollution event over Beijing-Tianjin-Hebei, China. *J. Environ. Sci.* **30**, 9–20 (2015).

38. Yao, D. et al. Oscillation cumulative volatile organic compounds on the northern edge of the North China Plain: impact of mountain-plain breeze. *Sci. Tot. Environ.* **821**, 153541 (2022).

39. Grant, E. R., Ross, A. N. & Gardiner, B. A. Modelling canopy flows over complex terrain. *Bound.-Layer. Meteorol.* **161**, 417–437 (2016).

40. Liu, S. et al. Numerical simulation for the coupling effect of local atmospheric circulations over the area of Beijing, Tianjin and Hebei province. *Sci. China Ser. D Earth Sci.* **52**, 382–392 (2009).

41. Forkel, R. et al. Analysis of the WRF-Chem contributions to AQMEII phase2 with respect to aerosol radiative feedbacks on meteorology and pollutant distributions. *Atmos. Environ.* **115**, 630–645 (2015).

42. Li, J. et al. Reinforcement of secondary circulation by aerosol feedback and PM2.5 vertical exchange in the atmospheric boundary layer. *Geophys. Res. Lett.* **48**, e2021GL094465 (2021).

43. Wang, N., Jiang, D. & Lang, X. Seasonality in the response of east asian westerly jet to the mid-holocene forcing. *J. Geophys. Res. Atmos.* **125**, e2020JD033003 (2020).

44. Zhong, Y. et al. Humidification of Central Asia and equatorward shifts of westerly winds since the late Pliocene. *Commun. Earth Environ.* **3**, 274 (2022).

45. Shapiro, M. A. Frontogenesis and geostrophically forced secondary circulations in the vicinity of jet stream-frontal zone systems. *J. Atmos. Sci.* **38**, 954–973 (1981).

46. IPCC. Working Group I Contribution to the IPCC Fifth Assessment Report Climate Change 2013: The Physical Science Basis, Summary for Policymakers (IPCC, Geneva, Switzerland, Final Draft; 2013).

47. Zhang, Q. et al. Asian emissions in 2006 for the NASA INTEX-B mission. *Atmos. Chem. Phys.* **9**, 5131–5153 (2009).

48. Blichner, S. M. et al. Process-evaluation of forest aerosol-cloud-climate feedback shows clear evidence from observations and large uncertainty in models. *Nat. Commun.* **15**, 969 (2024).

49. Ma, Z., Liu, R., Liu, Y. & Bi, J. Effects of air pollution control policies on PM_{2.5} pollution improvement in China from 2005 to 2017: a satellite-based perspective. *Atmos. Chem. Phys.* **19**, 6861–6877 (2019).

50. Ramanathan, V., Crutzen, P. J., Kiehl, J. T. & Rosenfeld, D. Aerosols, climate, and the hydrological cycle. *Science* **294**, 2119–2124 (2001).

51. Li, M. et al. MIX: a mosaic Asian anthropogenic emission inventory under the international collaboration framework of the MICS-Asia and HTAP. *Atmos. Chem. Phys.* **17**, 935–963 (2017).

52. Guenther, A. et al. Estimates of global terrestrial isoprene emissions using MEGAN (Model of Emissions of Gases and Aerosols from Nature). *Atmos. Chem. Phys.* **6**, 3181–3210 (2006).

53. Inness, A. et al. The MACC reanalysis: an 8 year data set of atmospheric composition. *Atmos. Chem. Phys.* **13**, 4073–4109 (2013).

54. Tang, G. et al. Impact of emission controls on air quality in Beijing during APEC 2014: lidar ceilometer observations. *Atmos. Chem. Phys.* **15**, 12667–12680 (2015).

55. Grell, G. A. et al. Fully coupled “online” chemistry within the WRF model. *Atmos. Environ.* **39**, 6957–6975 (2005).

56. Morrison, H., Thompson, G. & Tatarki, V. Impact of cloud microphysics on the development of trailing stratiform precipitation in a simulated squall line: comparison of one- and two-moment schemes. *Mon. Weather Rev.* **137**, 991–1007 (2009).

57. Iacono, M. J. et al. Radiative forcing by long-lived greenhouse gases: calculations with the AER radiative transfer models. *J. Geophys. Res.* **113**, <https://doi.org/10.1029/2008JD009944> (2008).

58. Jiménez, P. A. & Dudhia, J. Improving the representation of resolved and unresolved topographic effects on surface wind in the WRF model. *J. Appl. Meteorol. Climatol.* **51**, 300–316 (2012).

59. Tewari M. et al. Implementation and verification of the unified NOAH land surface model in the WRF model. In *Proc. 20th Conference on Weather Analysis and Forecasting/16th Conference on Numerical Weather Prediction*. pp.11–15 (2004).

60. Nakanishi, M. & Niino, H. An improved Mellor–Yamada level-3 model: its numerical stability and application to a regional prediction of advection fog. *Bound.-Layer. Meteorol.* **119**, 397–407 (2006).

61. Nakanishi, M. & Niino, H. Development of an improved turbulence closure model for the atmospheric boundary layer. *J. Meteorol. Soc. Jpn.* **87**, 895–912 (2009).

62. Grell, G. A. & Dévényi, D. A generalized approach to parameterizing convection combining ensemble and data assimilation techniques. *Geophys. Res. Lett.* **29**, 38–31–38–34 (2002).

63. Pfister, G. G. et al. CO source contribution analysis for California during ARCTAS-CARB. *Atmos. Chem. Phys.* **11**, 7515–7532 (2011).

64. Zaveri, R. A., Easter, R. C., Fast, J. D. & Peters, L. K. Model for Simulating Aerosol Interactions and Chemistry (MOSAIC). *J. Geophys. Res.* **113**, <https://doi.org/10.1029/2007JD008782> (2008).

65. Makar, P. A. et al. Feedbacks between air pollution and weather, part 2: Effects on chemistry. *Atmos. Environ.* **115**, 499–526 (2015).

66. Yahya, K., Wang, K., Zhang, Y. & Kleindienst, T. E. Application of WRF/Chem over North America under the AQMEII Phase 2 – Part 2: evaluation of 2010 application and responses of air quality and meteorology–chemistry interactions to changes in emissions and meteorology from 2006 to 2010. *Geosci. Model Dev.* **8**, 2095–2117 (2015).

67. Li, J. et al. WRF-Chem simulations of ozone pollution and control strategy in petrochemical industrialized and heavily polluted Lanzhou City, Northwestern China. *Sci. Total Environ.* **737**, 139835 (2020).

Acknowledgements

This work was jointly supported by the National Natural Science Foundation of China (42122034, 42075043), the Youth Innovation Promotion Association (2021427) and West Light Foundation (xbzg-zdysys-202215) of the Chinese Academy of Sciences, Key Talent Projects in Gansu Province, Central Guidance Fund for Local Science and Technology Development Projects in Gansu Province (No. 24ZYQA031), ACCC Flagship funded by the Academy of Finland grant number 337549 (UH), Academy professorship funded by the Academy of Finland (grant no. 302958), Academy of Finland projects no. 1325656, 311932, 334792, 316114, 325647, 325681, 347782, "Gigacity" project funded by Wihuri Foundation.

Author contributions

J.L., M.K., and J.M. designed the study. J.L., Y.H., R.D., B.Z., and H.L. performed the study. J.L., H.Y., T.V.K., Z.H., S.C., and S.T. analyzed data. J.L. and S.C. prepared figures. J.L., M.K., T.V.K., Z.H., K.T., and J.M. interpreted the results and wrote the paper. All authors participated in relevant scientific discussions and commented on the manuscript.

Competing interests

The authors declare no competing interest.

Additional information

Supplementary information The online version contains supplementary material available at

<https://doi.org/10.1038/s41612-024-00868-y>.

Correspondence and requests for materials should be addressed to Haipeng Yu.

Reprints and permissions information is available at <http://www.nature.com/reprints>

Publisher's note Springer Nature remains neutral with regard to jurisdictional claims in published maps and institutional affiliations.

Open Access This article is licensed under a Creative Commons Attribution-NonCommercial-NoDerivatives 4.0 International License, which permits any non-commercial use, sharing, distribution and reproduction in any medium or format, as long as you give appropriate credit to the original author(s) and the source, provide a link to the Creative Commons licence, and indicate if you modified the licensed material. You do not have permission under this licence to share adapted material derived from this article or parts of it. The images or other third party material in this article are included in the article's Creative Commons licence, unless indicated otherwise in a credit line to the material. If material is not included in the article's Creative Commons licence and your intended use is not permitted by statutory regulation or exceeds the permitted use, you will need to obtain permission directly from the copyright holder. To view a copy of this licence, visit <http://creativecommons.org/licenses/by-nc-nd/4.0/>.

© The Author(s) 2024